Time-Resolved Step-Scan Fourier Transform Infrared Spectroscopy of the CO Adducts of Bovine Cytochrome *c* Oxidase and of Cytochrome bo_3 from *Escherichia coli*†

James A. Bailey,‡ Farol L. Tomson,§ Sandra L. Mecklenburg,‡ Gina M. MacDonald,|| Andromachi Katsonouri,§ Anne Puustinen,⊥ Robert B. Gennis,§ William H. Woodruff,‡ and R. Brian Dyer*,‡

Los Alamos National Laboratory, Bioscience Division, Michelson Resource, Mail Stop J586, Los Alamos, New Mexico 87545, School of Chemical Sciences, University of Illinois, 600 South Mathews Street, Urbana, Illinois 61808, Department of Chemistry, James Madison University, 800 South Main Street, Harrisonburg, Virginia 22807, and Helsinki Bioenergetics Group, Institute of Biotechnology, P.B. 56, University of Helsinki, FI-00014, Finland

Received April 23, 2001; Revised Manuscript Received November 30, 2001

ABSTRACT: We have used cryogenic difference FTIR and time-resolved step-scan Fourier transform infrared (TR-FTIR) spectroscopies to explore the redox-linked proton-pumping mechanism of heme−copper respiratory oxidases. These techniques are used to probe the structure and dynamics of the heme a_3−Cu_B binuclear center and the coupled protein structures in response to the photodissociation of CO from heme Fe and its subsequent binding to and dissociation from Cu_B. Previous cryogenic (80 K) FTIR CO photodissociation difference results were obtained for cytochrome bo_3, the ubiquinol oxidase of *Escherichia coli* [Puustinen, A., et al. (1997) *Biochemistry 36*, 13195−13200]. These data revealed a connectivity between Cu_B and glutamic acid E286, a residue which has been implicated in proton pumping. In the current work, the same phenomenon is observed using the CO adduct of bovine cytochrome aa_3 under cryogenic conditions, showing a perturbation of the equivalent residue (E242) to that in bo_3. Furthermore, using time-resolved (5 μs resolution) step-scan FTIR spectroscopy at room temperature, we observe the same spectroscopic perturbation in both cytochromes aa_3 and bo_3. In addition, we observe evidence for perturbation of a second carboxylic acid side chain, at higher frequency in both enzymes at room temperature. The high-frequency feature does not appear in the cryogenic difference spectra, indicating that the perturbation is an activated process. We postulate that the high-frequency IR feature is due to the perturbation of E62 (E89 in bo_3), a residue near the opening of the proton K-channel and required for enzyme function. The implications of these results with respect to the proton-pumping mechanism are discussed. Finally, a fast loss of over 60% of the Cu_B−CO signal in bo_3 is observed and ascribed to one or more additional conformations of the enzyme. This fast conformer is proposed to account for the uninhibited reaction with O_2 in flow−flash experiments.

The heme−copper oxidases are a superfamily of enzymes whose task it is to reduce dioxygen to water and to convert the free energy from this reaction into a transmembrane protonmotive force (*1*, *2*). All of these enzymes have a heme−copper binuclear center, which is the active site where the dioxygen chemistry is catalyzed. In the bovine cytochrome *c* oxidase, the binuclear center consists of heme a_3 and Cu_B, whereas in cytochrome bo_3 from *Escherichia coli*, heme o_3 and Cu_B constitute the binuclear center. Of particular interest is the way in which the events at the active site are coupled to proton translocation within the enzyme and to electrogenic proton pumping (*1*, *3*−*6*). Fourier transform infrared (FTIR)[1] difference spectroscopy can identify changes that occur in the protein at the level of individual amino acid residues in response to changes in ligation and redox and protonation states (*7*−*10*). It is possible to correlate the observed spectroscopic changes with specific, functionally relevant structural features of the enzymes by combining the FTIR technique with site-directed mutagenesis and isotope labeling, guided by the high-resolution X-ray structural models of the cytochrome *c* oxidases from bovine heart (*11*, *12*) and from *Paracoccus denitrificans* (*13*, *14*) and the ubiquinol oxidase from *Escherichia coli* (*15*).

FTIR spectroscopy has already proven to be a powerful tool for exploring static structural features of the heme−copper respiratory oxidases (*16*−*21*). Such measurements were pioneered by Alben and his associates (*22*−*25*). The fully reduced enzyme forms a stable adduct with CO bound to the heme component of the binuclear center. Upon

† Work at Los Alamos National Laboratory was performed under the auspices of the U.S. Department of Energy. Supported by grants from the National Institutes of Health (GM45807 to W.H.W. and GM53640 to R.B.D.) and the U.S. Department of Energy (DEFG-02-87ER13716 to R.B.G.).

* Corresponding author. Phone: 505-667-4194; Fax: 505-667-0851; Email: bdyer@lanl.gov.

‡ Los Alamos National Laboratory.

§ University of Illinois.

|| James Madison University.

⊥ University of Helsinki.

[1] Abbreviations: FTIR, Fourier transform infrared; TR-FTIR, time-resolved Fourier transform infrared; MCT, mercury cadmium telluride.

10.1021/bi010823g CCC: $22.00
Published on Web 01/29/2002

photolysis, the FTIR studies showed that the CO is transferred from the heme Fe to Cu_B. At temperatures below 140 K, the Cu_B−CO adduct is a stable complex. Hence, spectra taken under cryogenic conditions in the dark (heme Fe−CO) and, then again, after photolysis (Cu_B−CO) reveal changes due simply to transferring the CO from one metal to the other, about 5 Å apart. This approach has been used to observe the relatively strong infrared absorption (1900−2200 cm^{-1}) due to CO itself as a probe to characterize the heme/copper center.

Recently, the FTIR difference approach has also been used to examine the photoperturbation difference spectrum throughout the mid-infrared region (1200−3200 cm^{-1}) of cytochrome bo_3 from *E. coli* (*18*). A key result of this work was the identification of an absorption band that shifts from about 1726 cm^{-1} to 1730 cm^{-1} upon photolysis. This feature has been assigned by comparison of site-directed mutants to the carboxylic acid C═O stretch of residue E286, which has been strongly implicated as being a key residue in the "D-channel," a proton pathway that is critical for the formation of intermediate P and subsequent steps coupled to proton pumping (*26*−*29*). The FTIR results clearly establish the protonation state of E286 in the fully reduced enzyme (protonated). Furthermore, the perturbation of the C═O stretch (of the −COOD side chain) of E286 upon CO photodissociation from the heme reveals a conformational connectivity between the CO ligation status of the heme/copper center and the environment sensed by E286 (*18*). It was suggested that the connectivity occurs through a hydrogen bond network that likely contains bound water molecules between E286 and a histidine ligand to Cu_B (*18*, *30*).

Changes in at least one carboxyl group, accompanying the full reduction of the oxidized enzyme, have also been identified by static FTIR difference spectroscopy. Hellwig et al. (*16*, *31*−*33*) examined changes in the spectrum upon electrochemical reduction of the heme−copper oxidases from a number of different organisms, whereas Lübben and Gerwert (*17*) examined the photochemical reduction of both cytochrome bo_3 from *E. coli* and the cytochrome *c* oxidase from *Rhodobacter sphaeroides*. In each of these cases, an absorption band shifts from higher frequency (about 1745 cm^{-1}) to lower frequency (1737−1732 cm^{-1}) upon full reduction of the enzyme. This has been interpreted as being due either to a proton transfer between two carboxyl groups (*16*) or possibly due to a shift of a protonated carboxyl group to a more hydrophilic environment (*17*). The aforementioned studies of CO photodissociation in the fully reduced enzymes strongly suggest that E286 (or its equivalent residue in other oxidases) is also responsible for the difference feature near 1735 cm^{-1} observed upon reduction of the heme−copper oxidases.

Time-resolved infrared approaches, generally using single-wavelength probe light in the CO frequency region (1900−2100 cm^{-1}), have been used to probe the dynamics of specific structural features of the heme−copper oxidases (*34*−*38*). For example, the dynamics and the structural progress of the heme/copper CO exchange reactions have been studied on picosecond and longer time scales (*34*−*37*). Infrared studies of oxidase dynamics would obviously be more informative if they could be applied to simultaneous observation of multiple wavelengths (as is the case for FTIR in static observations) rather than limited to single wavelengths. Recently, Rost et al. (*39*) have reported on a time-resolved FTIR study using a rapid-scanning technique (time resolution of 30 ms) of cytochrome *c* oxidase from *P. denitrificans* in both the fully reduced and mixed-valence forms. Here we report a multiwavelength IR study of oxidase dynamics, wherein we apply the technique of time-resolved step-scan FTIR with time resolution of 5 μs to the dynamics observable in the mid-IR spectra of cytochromes aa_3 (bovine) and bo_3 (*E. coli*). The time-resolved difference spectra are compared to the cryogenic difference spectra in both cases. We find evidence for the perturbation of multiple carboxylic acid IR absorbances following photodissociation of CO. The perturbation of the infrared spectral features arising from the carboxylic side chains in the time-resolved measurements reveals that the ligation reactions of the binuclear centers in both aa_3 and bo_3 are coupled to these proton-labile groups at room temperature. The implications of these results with respect to the proton-pumping mechanism are discussed.

MATERIALS AND METHODS

Sample Preparation. Bovine heart cytochrome oxidase and cytochrome bo_3 from *E. coli* were isolated and prepared as previously described (*37*, *40*). Each enzyme solution was 0.3−0.5 mM oxidase, 100 mM sodium phosphate buffer with 0.1% dodecyl maltoside at pH 7.4. Reduction was performed by the addition of sodium dithionite to the deaerated solution under an argon atmosphere. The carbonmonoxy derivatives were prepared by equilibration of 1 atm of CO with the solution of the reduced enzyme for 10−30 min. Exchange into D_2O was achieved by repeatedly concentrating the resting-state (oxidized) enzyme in an Amicon ultrafiltration cell with a 50 μm filter after dilution with D_2O buffer, until the solution was >99% D_2O.

FTIR Spectroscopy. The IR transmission sample cells consisted of CaF_2 windows with 15 or 25 μm Teflon spacers in demountable IR cell mounts. The assembled cells were purged with CO or Ar before filling as appropriate. Details of the time-resolved and cryogenic FTIR experiments are given in the following sections.

TR-FTIR. Time-resolved (TR) FTIR spectra were collected on a Bio-Rad FTS60A/896 Step-Scan Interferometer with adaptations as described below. A single laser pulse (Spectra Physics GCR-3 Nd:YAG; 532 nm; ca. 100−500 μJ; 10 ns duration) initiated the reaction at each mirror position. The interferometer stepping and laser firing both occurred at 10 Hz, with the interferometer serving as the master clock and the laser synchronized to fire once per interferometer step. A TTL pulse is generated by the interferometer at the start of each step cycle. This pulse is used to trigger a digital delay generator (Stanford Research Systems DG535) which then provides timing signals for the laser lamps and Q switch. The laser firing is delayed to near the middle of the 100 ms period between steps, to allow sufficient time for the moving mirror to settle. Transient decay traces were collected at each mirror position, resulting in a three-dimensional data set. Typically, 500−1000 time points at 5 μs intervals were collected as an average of 32−64 scans at 4 cm^{-1} resolution over a free spectral range of 3850 cm^{-1} (about 3−6 h collection time). For samples with a transient lifetime greater than milliseconds, consecutive spectra have been co-averaged to increase the signal-to-noise ratio.

TR-FTIR offers the advantages of spectral multiplexing, increased IR throughput, and relatively fast data acquisition over conventional point-by-point time-resolved IR techniques (*8*). To optimize the signal-to-noise ratio, the following adaptations have been incorporated into a Bio-Rad FTS60A/896 step-scan FTIR. The collimated IR beam from the interferometer is directed out of a sampling port to a turning mirror and then to a focusing lens. The IR beam is focused to a 300−1000 μm spot at the sample. The transmitted IR light is then collected and refocused by a single lens onto a photovoltaic mercury cadmium telluride (MCT) detector (Graseby IR, 2 mm element, 1 MHz bandwidth). A low-pass optical filter (<2250 cm^{-1}) and the CaF_2 lenses (>1150 cm^{-1}) restrict the usable bandwidth, but also increase the effective dynamic range of the detector. The entire external optical train is housed in a dry N_2-purged Plexiglas enclosure.

The Bio-Rad Win IR−Pro software program under Step-Scan TRS collect mode allows the amplified signal from the external detector to be passed directly back through the spectrometer for digitization and processing. The fastest sampling interval is 5 μs, limited by the digitization rate of the spectrometer's onboard A/D converter (200 kHz). Full transient decay traces were collected at each mirror position, resulting in a three-dimensional data set. Data collection was initiated before the laser fires to collect a series of reference spectra. The Bio-Rad step-scan instrument dithers the moving mirror to provide feedback control for mirror positioning. This dither produces an infrared transient (at the fixed frequency of the dither) which has a large amplitude compared to that of a typical laser-induced transient. The dither transient acts as a significant noise source unless it can be demodulated from the transient of interest. Demodulation of the dither transient is accomplished by precise control of the phase of the laser firing and data collection relative to the phase of the dither signal using the digital delay generator described above. Time-resolved difference absorbance spectra are computed as

$$\Delta A_t = -\log(S_{+t}/R_{-t})$$

where ΔA_t is the differential absorbance at time t (a multiple of the 5 μs sampling interval) after the laser excitation, and R and S are the single-beam absorbance spectra before ($-t$) and after ($+t$) the laser is fired, respectively. Thus, the dither signal is removed from each time-resolved difference spectrum by computing the ratio of spectra that are exactly matched in the phase and amplitude of the dither signal. Only a few cycles of the dither signal are actually sampled before t_0 in order to simplify the data handling; to sample the entire period of the dither (62.5 μs), using the 5 μs sampling interval, only 125 μs of reference data (25 spectra) is needed.

Cryogenic FTIR. Low-temperature spectra were collected on a Perkin-Elmer 1760x FTIR. Samples were mounted in an APD Cryogenics cryostat and maintained at 80 ± 0.2 K. Reference or "dark" spectra (64 scans) were collected at 4 cm^{-1} resolution immediately before photolysis. The sample was then photolyzed with one or two 10 ns pulses of 3 mJ, 532 nm Nd:YAG laser light, or 1−2 μs illumination at 2 mW from an Ar^+ laser, after which "light" spectra were collected (64 scans). Difference spectra (ΔA) were calculated directly by ratioing against the previous "dark" spectrum. The sample was warmed to ~250 K to allow CO to recombine with the heme, and then cooled again, and the experiment was repeated. Typically, 6−8 sets of 64 scans were co-averaged.

Difference FTIR spectroscopy of oxidase samples at cryogenic temperatures has several experimental requirements. The CO-ligated protein is highly photosensitive and undergoes irreversible photolysis at temperatures below 200 K. Therefore, light must be rigorously excluded from the sample compartment once the sample is frozen, and a germanium filter must be used to block the FTIR spectrometer's He−Ne alignment laser which otherwise passes through and photolyzes the sample. The high photosensitivity of the samples also means that it is possible to over-irradiate the protein, causing additional changes in the observed spectrum (i.e., the initial photoproduct is itself photolabile). To determine an appropriate excitation energy, a power dependence was performed on both the bovine cytochrome *c* oxidase and cytochrome bo_3. The dependence was determined for the percentage photolysis achieved with a series of 532 nm laser shots (1 mJ shots for the bovine enzyme; 90 μJ shots for cytochrome bo_3) on total laser power. With 5 mJ total energy, 80−85% photolysis is obtained, and this is true (within 5%) whether the energy is delivered as a single shot of 5 mJ or a number of shots of lower energy (e.g., 5 × 1 mJ). To avoid secondary photolysis, one or two shots of 3−5 mJ, 532 nm light were used in the experiments described herein. Finally, the temperature of the frozen sample must be precisely controlled (±0.2 °C or better) because the spectrum of the solvent varies with temperature and difference spectra show undesirable baseline fluctuations if excessive temperature variations occur during data collection.

RESULTS

The cryogenic (80 K) FTIR difference spectrum (light *minus* dark) of the CO adduct of fully reduced bovine cytochrome *c* oxidase is compared with the time-resolved spectrum (co-averaged first 125 μs after photodissociation) in Figure 1. The sharp trough at 1963.5 cm^{-1} is from CO bound to heme a_3, and is the dominant feature in both spectra. The smaller negative absorbance band at 1945 cm^{-1} in the cryogenic difference spectrum is due to the β-conformer of the oxidase, as previously described (*20*, *25*, *37*, *41*). The β-conformer is not as evident in the time-resolved (room temperature) spectrum, but compares well to photostationary spectra collected at room temperature as reported by Einarsdóttir et al. (*37*), who showed that the signal due to the heme-CO of the β-conformer shifts with temperature, starting at 1948 cm^{-1} at 21 K and shifting up to 1959 cm^{-1} at room temperature. At room temperature, the two heme−CO bands are overlapped and appear as a single feature with a broadened basal region. In the low-temperature spectrum shown in Figure 1, the peak at 2063 cm^{-1} is from CO bound to Cu_B. This absorption band is very weak in the time-resolved difference spectrum recorded at room temperature. It has been previously shown that at room temperature, the CO is transferred from the heme Fe to Cu_B in less than 1 ps (*35*−*37*), and that the rate of dissociation of CO from Cu_B to solution is 7×10^5 s^{-1} (*34*, *37*). Hence, the expectation is that CO will have dissociated from Cu_B within the first few microseconds and equilibrated with the CO in solution, which

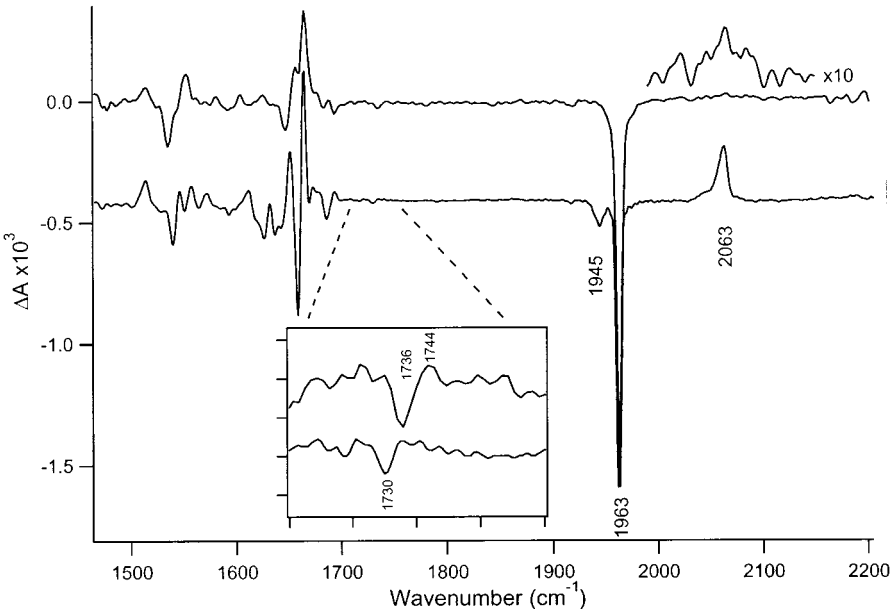

FIGURE 1: Comparison of the FTIR difference spectra of the CO adduct of the fully reduced bovine cytochrome *c* oxidase (cytochrome aa_3) following photolysis of the heme a_3 Fe−CO complex. Lower trace: cryogenic (80 K) light minus dark difference spectrum. Upper trace: step-scan time-resolved spectrum recorded at 295 K and co-averaged over the first 125 μs following photolysis. The weak Cu_B−CO peak at 2063 cm^{-1} in the time-resolved spectrum is shown on a 10 times expanded scale. Inset: lower left, expanded region showing the carboxylic acid features in both the 80 K (lower) and time-resolved, 295 K (upper) spectra.

is consistent with the spectrum shown in Figure 1. The equilibrium constant (87 M^{-1}) predicts that in the steady state 7−8% of the enzyme will have CO bound to Cu_B, but this small fraction is difficult to observe within the signal-to-noise of Figure 1. To discern the presence of the Cu_B−CO species, it is necessary to measure the integrated intensities of the heme− and Cu_B−CO regions in both the 80 K and the room-temperature spectra. Integration of the Cu_B−CO region of the room-temperature spectrum yields an intensity which is converted to a population by using the ratio of Cu_B−CO to heme−CO intensities at 80 K as a means to approximate ϵ_{Cu_B-CO} (100% Cu_B−CO). This analysis yields a room-temperature population of about 10% Cu_B−CO. Clearly, the room-temperature time-resolved FTIR spectrum in Figure 1 substantially represents the difference between the fully reduced bovine oxidase with CO bound to the heme Fe and the reduced enzyme with CO not bound to the enzyme, while the cryogenic spectrum represents the difference between the heme−CO and the Cu_B−CO species.

The time-resolved and cryogenic difference infrared spectra of aa_3 (and bo_3) show features whose absorbances (positive or negative) are on the order of 0.001 absorbance unit or less. The noise level in the cryogenic difference spectra is on the order of 5×10^{-6} (rms) absorbance unit, while the noise level in the time-resolved spectra is somewhat higher, on the order of 10^{-5} absorbance unit. The absorbance spectra from which the difference spectra are calculated have peak amide I absorbances near 1.0 absorbance unit (not shown). The sensitivity of the IR difference approach is further demonstrated, as we reported previously (*18*), by the presence of the ^{13}CO satellite on the low-energy side of the main Fe(C−O) absorbance, which is clearly visible in all of these spectra (1.1% of the total CO). Some of the smallest features, such as the carboxylic acid bands above 1700 cm^{-1}, are very weak, with a signal-to-noise ratio of 2−4. The limited signal-to-noise notwithstanding, these features are highly reproducible, even for different samples and different enzyme preparations. The spectra shown are the best of the 3−5 separate data sets obtained for each experiment.

There are evident differences in comparing the main features of the cryogenic and room-temperature spectra. Some of the differences between these two spectra result from the relatively narrower bands in the spectrum recorded at 80 K, but other differences must be due to the fact that in one case (80 K), the final state has CO bound to Cu_B, whereas in the other case (room temperature), CO has dissociated from the enzyme. In the cryogenic difference spectrum, a feature due to a change in absorbance of the C═O stretch of the carboxylic acid side chain of a glutamic or aspartic acid can be observed as predominantly a trough at 1730 cm^{-1} with a small positive band near 1734 cm^{-1} (Figure 1, inset). We assign this as the equivalent to the feature that we previously identified in cytochrome bo_3 originating from residue E286 (*18*), and is, therefore, attributed to a perturbation of the equivalent residue in the bovine oxidase, namely, E242. In the time-resolved (125 μs) spectrum, this feature is shifted slightly and broadened, and the positive component is significantly more prominent (Figure 1, inset). The time-resolved spectrum is essentially identical to the photostationary spectrum obtained by Rich et al. (*42*), in which the contribution of two different residues is inferred from the H/D isotope dependence of these features. The close correspondence of the time-resolved spectra reported here with the photostationary spectrum of Rich et al. implies the contribution of two different carboxylic acid groups in the time-resolved spectra at room temperature. These carboxylic acid features decay on a time-scale coincident with the recombination of CO to heme a_3. It is evident that there is a substantial perturbation of these carboxyl groups upon light-induced dissociation of CO from heme a_3 and ligation to Cu_B, but that persists well beyond the time scale of the dissociation of CO from Cu_B.

Figure 2 shows the time-resolved step-scan FTIR difference spectrum (1.2 ms) following photolysis of the CO

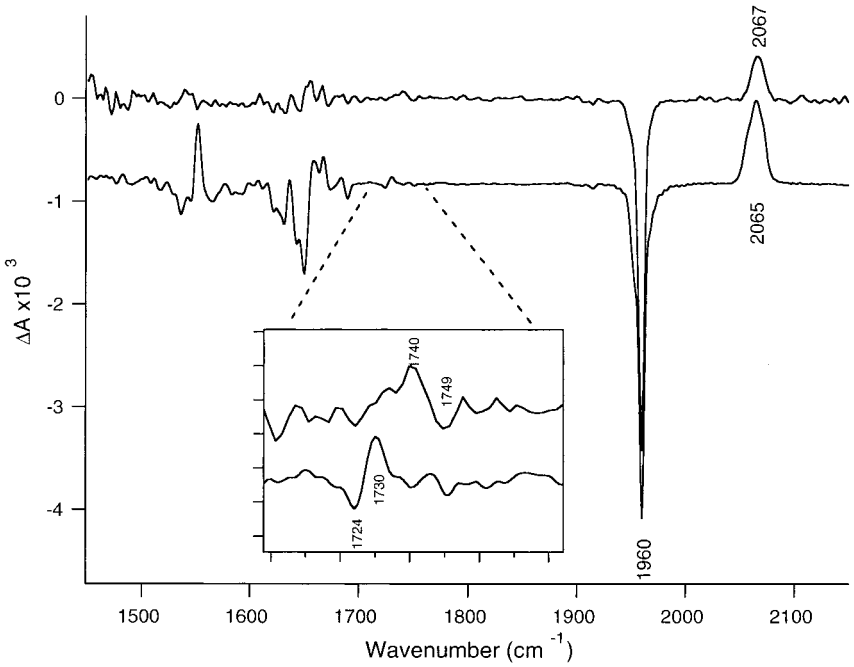

FIGURE 2: Comparison of the FTIR difference spectra of the CO adduct of the fully reduced *E. coli* cytochrome bo_3 following photolysis of the heme o_3 Fe−CO complex. Lower trace: cryogenic (80 K) light minus dark difference spectrum. Upper trace: time-resolved step-scan FTIR spectrum recorded at 295 K and at 1.2 ms following photolysis. Inset: expanded region showing the carboxylic acid features in both the 80 K (lower) and time-resolved, 295 K (upper) spectra.

adduct of cytochrome bo_3 at room temperature compared to the light-minus-dark spectrum of bo_3 recorded at 80 K. Again, the room-temperature and cryogenic spectra show significant differences. In cytochrome bo_3, the binding constant of Cu_B for CO (when CO is not bound to heme o_3) is substantially larger than that of cytochrome aa_3, such that CO occupies approximately 27% of the Cu_B sites during equilibrium rebinding (*43*). This is evident in the room-temperature trace, wherein Cu_B−CO is visible at 2067 cm^{-1} with appreciable intensity. However, full occupancy of Cu_B−CO produces a significantly larger band, as is seen in the 80 K spectrum. Comparison of the integrated intensities for these bands reveals a room-temperature occupancy of the Cu_B−CO state of about 29%, which is consistent with the measured K of 400 M^{-1} and the CO concentration of 1 mM. As in the aa_3 spectra, difference features in the amide and side chain regions (below 1800 cm^{-1}) are substantially more intense in the 80 K spectrum. This difference could be due to either narrower peak widths or greater occupancy of Cu_B in the 80 K spectrum. The E286 carboxyl C═O stretching band is seen as a derivative-shaped feature in both spectra with the trough/peak at room temperature at 1726/1732 cm^{-1} and at low temperature at 1724/1730 cm^{-1}. Analogous to aa_3, there is an additional feature in the room-temperature data, but clearly resolved in this case with a peak/trough at 1740/1749 cm^{-1}. The shape of the difference feature that we have associated with E286 in bo_3 (E242 in aa_3) is not invariant. Because the observed frequency shifts are smaller than the infrared peak widths of this residue (*18*), the shape of the difference feature is very sensitive to whether intensity, line width, frequency, or any combination of these change upon photolysis. Depending upon which of these change and in what direction, the difference feature can appear as a simple positive or negative peak, or as a first- or second-derivative-like line shape.

Rost et al. have recently obtained the redox difference FTIR spectra of *P. denitrificans* in both fully reduced and mixed-valence forms (*39*). They note that in the *Paracoccus* enzyme, there is no detectable signal due to E278 (corresponding to E242 in bovine and E286 in *E. coli*) following CO photolysis for the fully reduced form; however, this residue does give rise to a difference feature for the mixed-valence form. They conclude that the perturbation felt by E278 is caused by back-electron-transfer from heme a_3 to heme *a*, a process that does not occur in the fully reduced enzyme. As reported here, this is obviously not the case for either bovine aa_3 or bo_3 from *E. coli*.

The TR-FTIR spectra of cytochrome bo_3, taken at three discrete times after photodissociation (10, 70, and 385 μs), are shown in Figure 3. Analysis of these results suggests that cytochrome bo_3 does not behave as a single homogeneous population following photodissociation of CO, but that there are at least two populations with spectroscopically and kinetically distinct Cu_B−CO species. The inset in Figure 4 shows the initial Cu_B−CO peak centered at 2067 cm^{-1} decays within 20 μs to an intermediate spectrum with a slightly shifted center frequency (2070 cm^{-1}), which in turn decays to the steady-state rebinding fraction discussed above within 200 μs. Within this same early time, the carboxylic acid features are also diminished (Figure 3, inset) with concomitant evolution of band shape. Although there are very few time points covering the fastest decay, a rough estimate of the decay rate can be extracted by fitting a biexponential decay function to the integrated intensity of the Cu_B−CO band (Figure 4). Extrapolation of these results to zero time and peak integration yield the approximate fractions of total enzyme represented by these kinetic phases: 60% in the fast phase (∼70 000 s^{-1}); 13% in the intermediate phase (∼7000 s^{-1}); and 27% in the steady-state phase. While multiple kinetics phases are also seen in the CO rebinding reaction,

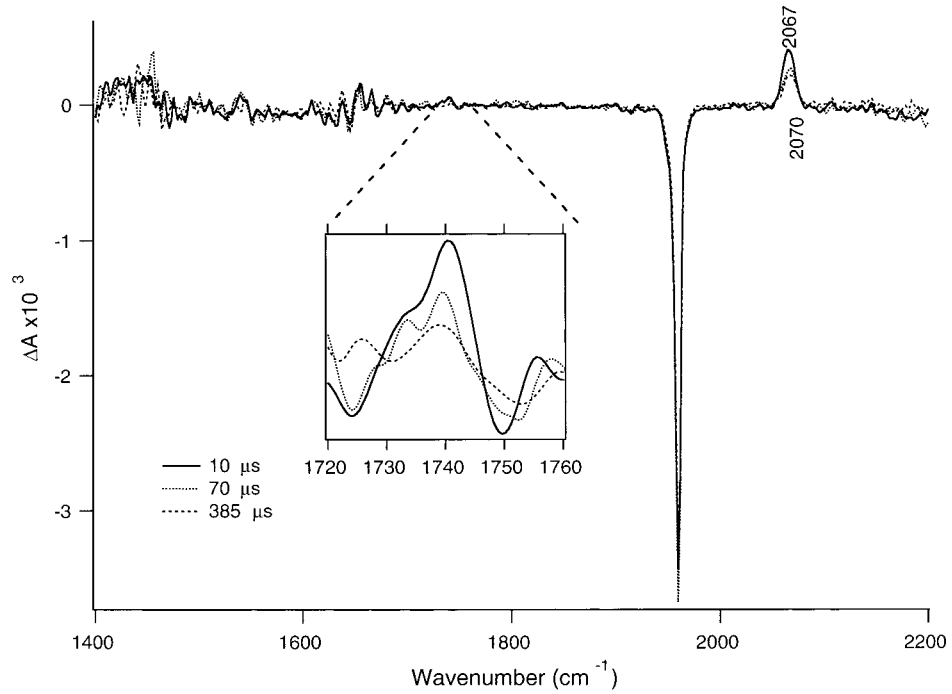

FIGURE 3: Time-resolved step-scan FTIR difference spectra of cytochrome bo_3 obtained at three times following photodissociation of CO at 300 K: solid trace, 10 μs; dashed trace, 70 μs; dotted trace, 385 μs. Inset: expanded region showing carboxylic acid features at the same three time points.

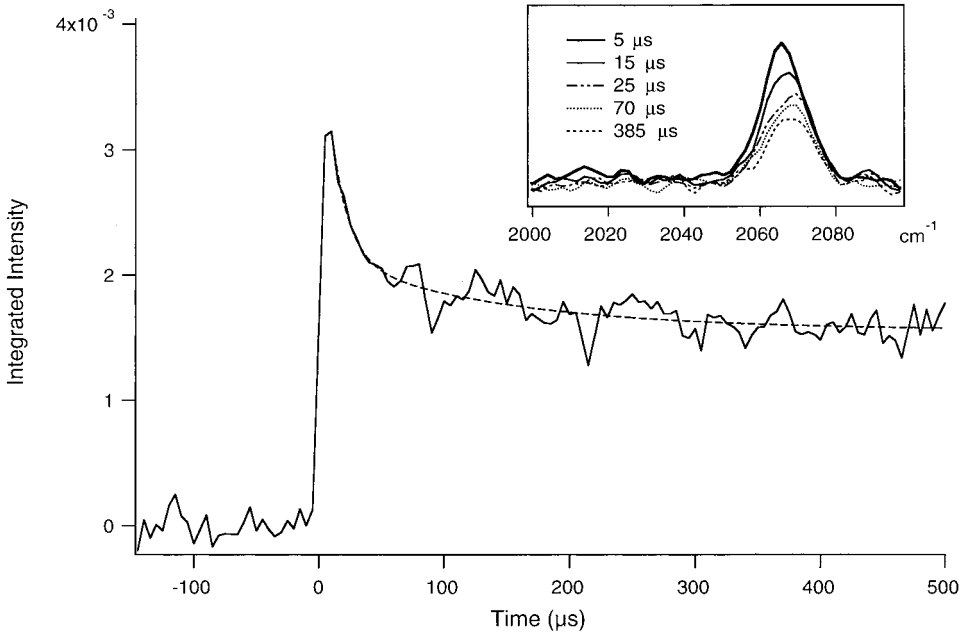

FIGURE 4: Integrated intensity of the Cu_B−CO band of cytochrome bo_3 vs time after photolysis of the heme−CO species. The dotted line represents the best fit of a biexponential decay function ($k_1 \sim 70\,000$ s^{-1}, $k_2 \sim 7000$ s^{-1}) with the intensity at long times representing the equilibrium Cu_B−CO occupancy before heme−CO rebinding occurs. Inset: spectra of the Cu_B−CO band from bo_3 at various times. Note the shift from 2067 to 2070 cm^{-1} within the initial fast (20 μs) decay.

previous saturation kinetic measurements show that none of these correspond to the rapid phase of CO dissociation from Cu_B following photolysis (*43*). In addition, the photostationary Cu_B−CO IR band shape most closely resembles the spectrum of the slowly dissociating conformer (in frequency and bandwidth), suggesting that the population of the Cu_B−CO form of the slowly dissociating conformer predominates at equilibrium. We conclude that the fast Cu_B−CO dissociation phase is due to a conformer that predominates in the Fe−CO and transient Cu_B−CO forms of bo_3 (on the microsecond time scale) but equilibrates to a minor fraction of the total by the time CO rebinding commences (milliseconds).

DISCUSSION

We have used time-resolved step-scan FTIR difference spectroscopy in the current work to examine the dynamics of the heme−copper oxidases. We have shown that the shifts in the IR signal from the glutamic acid residue E286 in cytochrome bo_3 from *E. coli*, which were previously observed

in the static difference spectra at 80 K, are also present in the time-resolved FTIR spectra at room temperature. Moreover, analogous features are observed in both the cryogenic and room-temperature time-resolved FTIR spectra of bovine cytochrome aa_3. The time-resolved measurements establish a connection between the ligation reactions of the binuclear center and the proton-labile side chain of E286 (E278, bovine) under functional conditions (i.e., room temperature). This residue has been implicated as a key feature of the redox-linked proton pump of the heme−copper oxidases. Recently, Backgren et al. (*5*) have shown that although this glutamic acid is highly conserved, it is not specifically required for enzyme activity. Mutant studies of the *P. denitrificans* enzyme in which E278 (equivalent to E286 in *E. coli*) and a neighboring glycine have been substituted show dramatically reduced activity, but further substitution of Phe-274 to tyrosine causes recovery of activity to nearly 10% of that of the wild type. This triple mutant mimics the structure of cytochrome caa_3 from *Rhodothermus marinus*, one of the few examples of a heme−copper oxidase that lacks the E278 equivalent. It is apparent that the oxidase enzymes require either a protonatable or at least a hydrophilic residue in this region of the protein to assist in establishing a pathway from the D-channel to the binuclear active site.

The time-resolved, step-scan FTIR measurements also reveal the dynamics of the ligation reactions at the binuclear center and the coupled protein response. In the current work, this technique was used to obtain spectra of the oxidases at room temperature with a time resolution of 5 μs and longer, both during (for cytochrome bo_3) and after (for both cytochromes bo_3 and aa_3) the dissociation of CO from Cu_B and its equilibration with solution, and before significant recombination with the heme has occurred. The averaged spectrum obtained in the first 125 μs following photolysis of the heme Fe−CO adduct of cytochrome aa_3 (upper trace in Figure 1) shows that the Cu_B−CO adduct has already reached its dissociative equilibrium (<10% Cu_B−CO, 2063 cm^{-1} region) in the bovine enzyme and that a perturbed carboxylic acid feature is still visible at 1736/1744 cm^{-1}. Hence, the persistent change in environment sensed by the carboxyl in the *bovine* enzyme must be due to some effect in addition to the formation of the Cu_B−CO adduct, because this effect persists after Cu_B−CO has dissociated. The situation is not so clear in the case of bo_3, because although there is some decay of the initial amplitude of the carboxylic acid features (Figure 3, inset), there may also be a persistent component that is difficult to distinguish from that due to the large steady-state population of the Cu_B−CO form of the protein. In addition, we cannot rule out the possibility that an analogous initial decay of the carboxylic acid features in aa_3 occurs during the dissociation of CO from Cu_B (1.5 μs half-life), because this process is complete before our earliest measurement (5 μs).

There are a number of possible explanations for the persistence of the carboxylic acid features. The most likely scenario in our view is that the binding of CO to Cu_B triggers a change in the protein structure that persists for relatively long times (several milliseconds) after dissociation of the Cu_B−CO adduct. This change could be a loss of one of the histidine ligands to Cu_B or a rotation of the side chain conformation of the glutamic acid, either of which could have an activation energy for reversal following the departure of CO from Cu_B. In contrast, the fraction of the perturbation that decays with the loss of CO from Cu_B is likely due at least in part to an inductive effect of CO bound to Cu_B, through a direct hydrogen-bonded pathway as proposed previously (*18*).

Recent work by Rich et al. (*42*) has demonstrated that for aa_3 there are two different glutamic acid residues that are perturbed by CO photolysis. The time-resolved aa_3 spectra presented here closely match the photostationary spectra obtained by Rich et al. for the protein in D_2O (*42*). The photostationary spectra have been shown to have contributions from two different residues based on H/D isotope exchange experiments, a low-frequency component near 1735/1742 cm^{-1} (deuterated, i.e., −COOD) and a higher frequency component (not deuterated, i.e., exchange-inaccessible). Furthermore, the spectrum at low temperature obtained in the present work clearly contains only the lower frequency component. The higher frequency component must be due to an activated process, such as a conformational change of the protein, which is not accessible at low temperature (80 K). The analogous two components are observed for bo_3 albeit at slightly different frequencies. Both a low-frequency (1726/1732 cm^{-1}) and a high-frequency (1740/1749 cm^{-1}) component are observed in the time-resolved spectra of bo_3, but only the low-frequency component is observed at low temperature (Figure 2, inset). The low-frequency component has been assigned to E286 on the basis of site-directed mutagenesis studies (*18*). The high-frequency component was not observed previously, because the spectra were all obtained at low temperature. It is likely that the low-frequency signal in aa_3 (the exchange-accessible residue) is due to the analogous residue (E242), and that the higher frequency component (exchange-inaccessible) corresponds to the analogous high-frequency component in bo_3.

The identity of the residue responsible for the high-frequency signals in both the bovine and *E. coli* enzymes is unknown, but it must be a *protonated* carboxyl residue and therefore must have an unusually high pK_a as a consequence of being buried within the protein and protected from the solvent. In addition, the higher frequency means a stronger C═O bond and therefore weaker H-bonding to surrounding groups or structural water. There are only a limited number of possibilities that meet these conditions based on inspection of the crystal structure of the bovine oxidase, namely, residues $E62^{II}$ (aa_3 sequence, subunit II), $E90^{III}$, $D246^{III}$, $D51^{I}$, and the heme propionates. The residues in subunit III seem unlikely candidates, as this subunit has been shown to be unnecessary for enzyme activity (*44*), and therefore unlikely to be perturbed by events at the catalytic site. $D51^{I}$ is part of a possible proton channel proposed by Yoshikawa et al. (*45*), who have suggested that it is protonated in the fully reduced enzyme. This residue is glycine in bo_3, however, which eliminates it as the source of the analogous features in the two enzymes. The IR frequencies of the heme propionates in *Paracoccus denitrificans* cytochrome *c* oxidase have been established using specific ^{13}C labeling and FTIR difference spectroscopy (*33, 46*). An infrared band at 1676 cm^{-1} has been assigned to the COOH mode of protonated heme propionate, eliminating it as the source of the high-frequency feature. $E62^{II}$ sits near the entrance of the K channel and is shielded from water, and hence would likely have a protonated, weakly H-bonded carboxyl group,

consistent with the observed high-frequency IR feature. Mutation of the corresponding residue in bo_3 ($E89^{II}$) has been shown to reduce turnover by as much as 90% (*47*). Also, electrostatic calculations have suggested that there is sizable coupling between the corresponding residue $E78^{II}$ of the *Paracoccus denitrificans* oxidase to $K354^{I}$ (K channel) and to the binuclear site and that there is significant change in the degree of protonation of this residue with redox state, approaching 80% in the fully reduced enzyme (*48*). Site-directed mutagenesis studies will be required to definitively assign the high-frequency IR feature, but the weight of the present evidence suggests that it is $E62^{II}$ ($E89^{II}$ in bo_3).

The observation of a second proton-labile group connected to the binuclear center is important regardless of its assignment. The connection could be via a direct H-bonded network whereby the change in ligation state of the binuclear center is transmitted as a change in the H-bonding to the carboxyl side chain. Alternatively, the connection could be more indirect, via a conformational change that affects either the electrostatic environment of the carboxyl side chain or the H-bonding, or both. Moreover, the connection between the sites is via an activated process that can be frozen out at 80 K. In contrast, the perturbation of the low-frequency feature due to $E242^{I}$ ($E286^{I}$ in bo_3) occurs even at 30 K and must therefore be activationless. This means that the coupling of the active site to two possible proton channels (the D channel containing E242 and the K channel having E62 near its entry) to the active site is fundamentally different. Interestingly, the delivery of protons to the heme−copper center apparently goes via different routes prior to (K-channel) and following (D-channel) the binding of dioxygen to the binuclear center (*29*). A protein conformational change has been suggested as a molecular switch of the preferred pathway for proton delivery (*29*). A molecular switch such as this could be triggered by the interaction of dioxygen either with heme a_3 Fe or with Cu_B, and hence could be related to the IR perturbations observed in the current work.

Another conclusion from this work concerns the dynamics of CO dissociation from the enzyme in cytochrome bo_3. Previous studies of CO photodissociation of the heme−copper oxidases have demonstrated that following photolysis, CO forms an obligate complex with Cu_B prior to equilibration with CO in the bulk solution (*35*, *37*, *43*, *49*, *50*). However, the microscopic rate constants describing the association and dissociation rate constants as well as the binding constant for the Cu_B−CO adduct vary widely in different oxidases (*43*, *49*, *50*). Kinetic modeling, for example, has shown that at room temperature the dissociation rate constant for Cu_B−CO is 7×10^5 s^{-1} for bovine aa_3 and 500 s^{-1} for bo_3 from *E. coli*, and is very small for the ba_3-type oxidase from *Thermus thermophilus* (*37*, *43*, *49*, *50*). The current work confirms that the Cu_B−CO adduct of cytochrome bo_3 is indeed, at a substantial level of occupancy, long-lived, and can be observed spectroscopically several milliseconds following photolysis by time-resolved step-scan FTIR difference spectroscopy. The fraction of occupancy of Cu_B−CO at long times is approximately the same as the persistent population of the shifted E286 signal in cytochrome bo_3.

Previous data obtained with the bovine oxidase are consistent with the requirement that the Cu_B−CO adduct dissociates prior to the reaction with dioxygen (*51*). There are numerous reports (*26*, *52*−*54*) of dioxygen reacting with fully reduced cytochrome bo_3 with half-times well below 1 ms following photolysis of the heme Fe−CO complex (i.e., flow−flash experiments), which would appear to be inconsistent with the long-lived Cu_B−CO adduct in this enzyme (Figure 2). It is obviously important to reconcile these observations. Our analysis of the time-resolved FTIR spectra following photolysis of the CO adduct of cytochrome bo_3 shows that there are distinct populations of the enzyme with very different rates of dissociation of the Cu_B−CO adduct and different Cu_B−CO vibrational frequencies. The existence of a population representing some 60% of the enzyme in the post-photodissociation reaction, wherein CO is entirely dissociated from Cu_B within 20 μs, is sufficient to explain the apparent discrepancies between the flow−flash oxygenation experiments and the saturation kinetics behavior of the CO rebinding reaction. The substantial population of the fast CO dissociating conformer should allow uninhibited access of O_2 to the active site.

REFERENCES

1. Ferguson-Miller, S., and Babcock, G. T. (1996) *Chem. Rev. 7*, 2889−2907.
2. Garcia-Horsman, J. A., Barquera, B., Rumbley, J., Ma, J., and Gennis, R. B. (1994) *J. Bacteriol. 176*, 5587−5600.
3. Rich, P. R., Jünemann, S., and Meunier, B. (1998) *J. Bioenerg. Biomembr. 30*, 131−138.
4. Wikström, M., Morgan, J. E., Hummer, G., Woodruff, W. H., and Verkhovsky, M. I. (1997) *Biological Spectroscopy, Part B*, Elsevier/North-Holland, Inc., New York.
5. Backgren, C., Hummer, G., Wikstrom, M., and Puustinen, A. (2000) *Biochemistry 39*, 7863−7867.
6. Rich, P. R., Breton, J., Junemann, S., and Heathcote, P. (2000) *Biochim. Biophys. Acta 1459*, 475−480.
7. Hienerwadel, R., Grzybek, S., Fogel, C., Kreutz, W., Okamura, M. Y., Paddock, M. L., Breton, J., Nebedryk, E., and Mäntele, W. (1995) *Biochemistry 34*, 2832−2843.
8. Slayton, R. M., and Anfinrud, P. A. (1997) *Curr. Opin. Struct. Biol. 7*, 717−721.
9. Troullier, A., Gerwert, K., and Dupont, Y. (1996) *Biophys. J. 71*, 2970−2983.
10. Zhang, H., Razeghifard, M. R., Fischer, G., and Wydrzynski, T. (1997) *Biochemistry 36*, 11762−11768.
11. Tsukihara, T., Aoyama, H., Yamashita, E., Takashi, T., Yamaguichi, H., Shinzawa-Itoh, K., Nakashima, R., Yaono, R., and Yoshikawa, S. (1996) *Science 272*, 1136−1144.
12. Tsukihara, T., Aoyama, H., Yamashita, E., Tomizaki, T., Yamaguchi, H., Shinzawa-Itoh, K., Nakashima, T., Yaono, R., and Yoshikawa, S. (1995) *Science 269*, 1069−1074.
13. Ostermeier, C., Harrenga, A., Ermler, U., and Michel, H. (1997) *Proc. Natl. Acad. Sci. U.S.A. 94*, 10547−10553.
14. Iwata, S., Ostermeier, C., Ludwig, B., and Michel, H. (1995) *Nature 376*, 660−669.
15. Abramson, J., Riistama, S., Larsson, G., Jasaitis, A., Svensson-Ek, M., Laakkonen, L., Puustinen, A., Iwata, S., and Wikström, M. (2000) *Nat. Struct. Biol. 7*, 910−917.
16. Hellwig, P. (1996) *FEBS Lett. 385*, 53−57.
17. Lübben, M., and Gerwert, K. (1996) *FEBS Lett. 397*, 303−307.
18. Puustinen, A., Bailey, J. A., Dyer, R. B., Mecklenburg, S. L., Wikström, M., and Woodruff, W. H. (1997) *Biochemistry 36*, 13195−13200.
19. Park, S., Pan, L. P., Chan, S. I., and Alben, J. O. (1996) *Biophys. J. 71*, 1036−1047.
20. Mitchell, D. M., Shapleigh, J. P., Archer, A. M., Alben, J. O., and Gennis, R. B. (1996) *Biochemistry 35*, 9446−9450.
21. Hosler, J. P., Shapleigh, J. P., Mitchell, D. M., Kim, Y., Pressler, M., Georgiou, C., Babcock, G. T., Alben, J. O., Ferguson-Miller, S., and Gennis, R. B. (1996) *Biochemistry 35*, 10776−10783.

22. Alben, J. O., Moh, P. P., Fiamingo, F. G., and Altschuld, R. A. (1981) *Proc. Natl. Acad. Sci. U.S.A. 78*, 234−237.
23. Alben, J. O., Altschuld, R. A., Fiamingo, F. G., and Moh, P. P. (1982) *Electron Transport and Oxygen Utilization*, Elsevier/North-Holland, Inc., New York.
24. Fiamingo, F. G., Altschuld, R. A., Moh, P. P., and Alben, J. O. (1982) *J. Biol. Chem. 257*, 1639−1650.
25. Fiamingo, F. G., Altschuld, R. A., and Alben, J. O. (1986) *J. Biol. Chem. 261*, 12976−12987.
26. Watmough, N. J., Katsonouri, A., Little, R. H., Osborne, J. P., Furlong-Nickels, E., Gennis, R. B., Brittain, T., and Greenwood, C. (1997) *Biochemistry 36*, 13736−13742.
27. Verkhovskaya, M. L., Garcia-Horsman, A., Puustinen, A., Rigaud, J. L., Morgan, J. E., Verkhovsky, M. I., and Wikström, M. (1997) *Proc. Natl. Acad. Sci. U.S.A. 94*, 10128−10131.
28. Ädelroth, P., Ek, M. S., Mitchell, D. M., Gennis, R. B., and Brzezinski, P. (1997) *Biochemistry 36*, 13824−13829.
29. Konstantinov, A. A., Siletsky, S., Mitchell, D., Kaulen, A., and Gennis, R. B. (1997) *Proc. Natl. Acad. Sci. U.S.A. 94*, 9085−9090.
30. Riistama, S., Hummer, G., Puustinen, A., Dyer, R. B., Woodruff, W. H., and Wikström, M. (1997) *FEBS Lett. 414*, 275−280.
31. Helwig, P., Soulimane, T., Buse, G., and Mantele, W. (1999) *FEBS Lett. 458*, 83−86.
32. Hellwig, P., Soulimane, T., Buse, G., and Mantele, W. (1999) *Biochemistry 38*, 9648−9658.
33. Hellwig, P., Grzybek, S., Behr, J., Ludwig, B., Michel, H., and Mantele, W. (1999) *Biochemistry 38*, 1685−1694.
34. Dyer, R. B., Einarsdóttir, O., Killough, P. M., López-Garriga, J. J., and Woodruff, W. H. (1989) *J. Am. Chem. Soc. 111*, 7651−7659.
35. Dyer, R. B., Peterson, K. A., Stoutland, P. O., and Woodruff, W. H. (1991) *J. Am. Chem. Soc. 113*, 6276−6277.
36. Dyer, R. B., Peterson, K. A., Stoutland, P. O., and Woodruff, W. H. (1994) *Biochemistry 33*, 500−507.
37. Einarsdóttir, O., Dyer, R. B., Lemon, D. D., Killough, P. M., Hubig, S. M., Atherton, S. J., Lopez-Garriga, J. J., Palmer, G., and Woodruff, W. H. (1993) *Biochemistry 32*, 12013−12024.
38. Iwase, T., Varotsis, C., ShinzawaItoh, K., Yoshikawa, S., and Kitagawa, T. (1999) *J. Am. Chem. Soc. 121*, 1415−1416.
39. Rost, B., Behr, J., Hellwig, P., Richter, O. M. H., Ludwig, B., Michel, H., and Mantele, W. (1999) *Biochemistry 38*, 7565−7571.
40. Rumbley, J. N., Nickels, E. F., and Gennis, R. B. (1997) *Biochim. Biophys. Acta 1340*, 131−142.
41. Fiamingo, F. G., Jung, D. W., and Alben, J. O. (1990) *Biochemistry 29*, 4627−4633.
42. Rich, P. R., and Breton, J. (2001) *Biochemistry 40*, 6441−6449.
43. Lemon, D. D., Calhoun, M. W., Gennis, R. B., and Woodruff, W. H. (1993) *Biochemistry 32*, 11953−11956.
44. Hendler, R. W., Pardhasaradhi, K., Reynafarje, B., and Ludwig, B. (1991) *Biophys. J. 60*, 415−423.
45. Yoshikawa, S., ShinzawaItoh, K., Nakashima, R., Yaono, R., Yamashita, E., Inoue, N., Yao, M., Fei, M. J., Libeu, C. P., Mizushima, T., Yamaguchi, H., Tomizaki, T., and Tsukihara, T. (1998) *Science 280*, 1723−1729.
46. Behr, J., Michel, H., Mäntele, W., and Hellwig, P. (2000) *Biochemistry 39*, 1356−1363.
47. Ma, J. X., Tsatsos, P. H., Zaslavsky, D., Barquera, B., Thomas, J. W., Katsonouri, A., Puustinen, A., Wikstrom, M., Brzezinski, P., Alben, J. O., and Gennis, R. B. (1999) *Biochemistry 38*, 15150−15156.
48. Kannt, A., Lancaster, C. R. D., and Michel, H. (1998) *Biophys. J. 74*, 708−721.
49. Woodruff, W. H., Dyer, R. B., and Einarsdottir, O. (1993) in *Biomolecular Spectroscopy* (Clark, R. J. H., and Hester, R. E., Eds.) pp 189−233, John Wiley & Sons Ltd., London.
50. Einarsdóttir, O., Killough, P. M., Fee, J. A., and Woodruff, W. H. (1989) *J. Biol. Chem. 264*, 2405−2408.
51. Bailey, J. A., James, C. A., and Woodruff, W. H. (1996) *Biochem. Biophys. Res. Commun. 220*, 1055−1060.
52. Puustinen, A., Verkhovsky, M. I., Morgan, J. E., Belevich, N. P., and Wikström, M. (1996) *Proc. Natl. Acad. Sci. U.S.A. 93*, 1545−1548.
53. Orii, Y., Mogi, T., Kawasaki, M., and Anraku, Y. (1994) *FEBS Lett. 352*, 151−154.
54. Wang, J., Rumbley, J., Ching, Y. C., Takahashi, S., Gennis, R. B., and Rousseau, D. L. (1995) *Biochemistry 34*, 15504−15511.

BI010823G